On the processing conditions and interfacial chemistry of composite PZT thick films on platinised silicon substrates

Journal Item

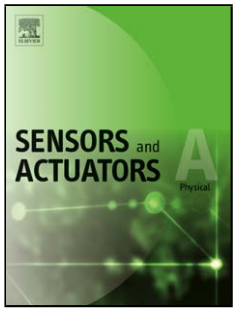

Title: On the Processing Conditions and Interfacial Chemistry of Composite PZT Thick Films on Platinised Silicon Substrates

Authors: R.D. Haigh, R.W. Whatmore

PII: S0924-4247(09)00119-8
DOI: doi:10.1016/j.sna.2009.02.037
Reference: SNA 6558

To appear in: *Sensors and Actuators A*

Received date: 9-8-2007
Revised date: 17-2-2009
Accepted date: 22-2-2009

Please cite this article as: R.D. Haigh, R.W. Whatmore, On the Processing Conditions and Interfacial Chemistry of Composite PZT Thick Films on Platinised Silicon Substrates, *Sensors and Actuators: A Physical* (2008), doi:10.1016/j.sna.2009.02.037

On the Processing Conditions and Interfacial Chemistry of Composite PZT Thick Films on Platinised Silicon Substrates

R.D. Haigh[1,*] and R.W. Whatmore[2]

[1] *Materials Engineering Group, Faculty of Mathematics Computing & Technology, The Open University, Walton Hall, Milton Keynes, Buckinghamshire, MK7 6AA, United Kingdom.*

[2] *Tyndall Institute, Lee Maltings, Prospect Row, Cork, Ireland.*

Received 9th August 2007, revised 17th February 2009 and accepted 22nd February 2009.

*Corresponding author. Tel.: +44-1908-332992; Fax: +44-1908-653858
E-mail address: r.haigh@open.ac.uk (R.D. Haigh)

Introduction

In recent years the use of ferroelectric thin films of $PbZr_xTi_{1-x}O_3$ (PZT) family for memory, piezoelectric and pyroelectric devices has drawn considerable interest. Thin film materials (<1 μm), which can be deposited onto platinised silicon for integration with microelectronic devices, have limited power output. Thick film materials (>10 μm) such as those from screen printing on to planar substrates yield greater power outputs, but are less conformal and suffer from greater surface roughness. Composite slurries can be derived from the dispersion of ceramic powders in metalorganic sols through spin casting or dip coating onto planar substrates. These films have intermediate properties between thin films and screen printed thick films. In the case of composite PZT thick films, for example, the surface roughness and bulk electrical properties can approach those of thin films and screen printed thick films respectively. Following deposition the thick film, screen printed or composite, is typically sintered at temperatures from 700 °C to 800 °C. However, film/substrate adhesion remains a difficulty when sintering at high temperatures and under differing sintering gasses.

PZT is a mechanically hard and chemically inert material and is therefore a difficult material to pattern; patterning of PZT thick films is essential to yield working devices. Therefore the difficulty is in obtaining dense, conformal PZT thick films with thicknesses between 1 to 10 μm with a low surface roughness; these films must exhibit good adhesion to the substrate and it must be possible to pattern these films in order to achieve working devices.

The composite slurry approach was first proposed with ultrasonically assisted dispersion of the ceramic powder [1], and later with ball milling of sub micron powders [2]. Low sintering temperatures (≤710 °C) have been achieved by incorporating a $PbO\text{-}Cu_2O$ (5% weight PZT powder) eutectic sintering aid into the slurry [2]; however, all of these films exhibited a high degree of porosity. An infiltration route has been employed to aid densification in which the sol was used to infiltrate the pores of the thick film. The infiltration route was proposed independently by two authors: Haigh [3] (received 2nd, May, 2000 and published June 2001) and Ohno [4] (received 12th, May, 2000 and published June 2000).

PZT thick films have also been prepared by the dispersion of nano and sub-micron powders in sols [5] and xerogels [6] respectively. Dip coating of planar substrates in a composite slurry followed by a sol infiltration step has yielded dense thick films with a smooth surface finish [7].

A particular problem with composite thick films is the tendency of the film to delaminate from the substrate. In this work it will be shown that this is due to the diffusion of Pb from the film into the substrate to flux with the Si.

Patterning of PZT thick films has been reviewed by Dorey and Whatmore [8] in which it has been claimed that lead diffusion barriers were introduced of the form TiO_2 [9] and YSZ [10] onto which PZT thick films were prepared. There was, however no mention of the YSZ process in the earlier paper by Wilson et al [10]. Indeed the earlier paper

presented no details of the processing of thermal barrier coatings for PZT thick films. This work was first presented in [11] (received 26th, April, 2004 and published June 2006) and will be presented in this paper. Details of Thick films on Si_3N_4 coated Si substrates incorporating a thick SiO_2(350 nm)/Ti/Pt(200-300 nm) layer [12] and a non-doped silicon glass barrier layer [13] have since been published; however, there has been no discussion of the interfacial reactions taking place during delamination of infiltrated PZT thick films in the literature.

The infiltration route may be described by a notation introduced in (1) below. Sol and composite layers were denoted as S and C respectively and introduced in the order from left to right as shown in (1):

$$\left[S_v^{\alpha 1,\alpha 2\ldots\alpha n} + n(C_\omega^{\beta 1,\beta 2\ldots\beta n} + mS_v^{\alpha 1,\alpha 2\ldots\alpha n}) + C_\omega^{\beta 1,\beta 2\ldots\beta n}\right]_b^a \quad \textbf{(1)}$$

The letters n and m are integers; a and b are the sintering temperature and sintering gas respectively. Heat treatments applied to each layer are denoted as α_i=α1, α2…αn and β_j=β1, β2…βn. Each thermal treatment corresponds to $\alpha i=T_i/t_i$ and $\beta j=T_j/t_j$ where T and t are temperature and time respectively. The spinning speed is denoted in subscripts as v and ω where v=ω=2000rpm/30s. The convention used in this paper is that $\alpha_i=\beta_j$ where α_1=200°C/50s and α_2=450°C/15s unless otherwise stated. The convention used in this paper is to express equation (1) in the order of C and S, but to omit the symbols α, β, v and ω.

We have reported PZT films of the form in equation (1) previously [3] where n=7, m=5, α1=200°C/50s α2=0, β1=0, β2=450°C/15s, b=Ar and a=710°C/30min; a polished cross section is shown in Fig 1 a. This film exhibited both glass like layers between the *C* layers and a discontinuous back electrode. The back electrode was a Pb_x-Pt_y intermetallic composed of PtPb with Pt_3Pb islands. Fig 1 b shows a film made under similar conditions, but with n=m=1. No glass like layers were shown in this film indicating that for small values of m the sol was infiltrated into the pores of the film. The glassy layers shown in Fig 1 a are thought to seal the film by lowering po_2 at the electrode substrate interface. Sintering under Ar combined with the effect of sealing the film is thought to have resulted in an abnormally low po_2 at the electrode substrate interface thereby preventing re-oxidation of the intermetallic.

In a reducing atmosphere the PZT can act as an oxygen source according to equation (2) [14] where the PbO component is reduced to atomic lead:

$$PbZr_xTi_{1-x}O_3 \longleftrightarrow PbO + yZrTiO_4 + zZrO_2 + wTiO_2 \quad \textbf{(2)}$$

$$PbO(s) \longleftrightarrow Pb(l) + \tfrac{1}{2}O_2(g)$$

$$PbO(s) \longleftrightarrow Pb(g) + \tfrac{1}{2}O_2(g)$$

$$ZrO_2(s) \longleftrightarrow ZrO_{2-x} + \tfrac{x}{2}O_2(g)$$

$$TiO_2(s) \longleftrightarrow TiO_{2-x} + \tfrac{x}{2}O_2(g)$$

In equation (2) oxygen is consumed by a source of residual carbon [14] according to equations (3) to (5) where equation (3) will be the case for low po_2.

$$C(s) + \tfrac{1}{2}O_2(g) \longleftrightarrow CO(g) \quad \textbf{(3)}$$

$$C(s) + O_2(g) \longleftrightarrow CO_2(g) \quad \textbf{(4)}$$

$$CO(g) + \tfrac{1}{2}O_2(g) \longleftrightarrow CO_2(g) \quad \textbf{(5)}$$

In the case of PZT thick films, such as those in Fig 1 a, a PbO-Cu_2O eutectic sintering aid was employed. In such films an excess of PbO exists, and it is considered unlikely that the PZT will be reduced in preference to PbO. Residual carbon arising from incomplete film pyrolysis is the most likely source of carbon for equations (3) to (5) for PZT thick films. It follows from the excess of PbO in the sintering aid that there will be an abundance of atomic Pb to yield the Pt_xPb intermetallic [3] according to equation (6):

$$Pb(l) + xPt(s) \longleftrightarrow Pt_xPb(s) \quad \textbf{(6)}$$

Brooks et al [15] have observed the formation and re-oxidation of a Pt_xPb intermetallic phase under Ar and air atmosphere at 460 °C, in sol-gel derived PZT thin films on Pt/Ti/SiO_2/Si substrates. The intermetallic was completely re-oxidised to Pt + PbO in an O_2 atmosphere at the same temperature.

Screen printed PZT thick films prepared on Pt/Ti/SiO_2/Si substrates and fired at 800 °C under an air atmosphere (high po_2) have exhibited damaged back electrodes [16, 17]; the electrode was swollen and had delaminated from the substrate, but not from the PZT. Bubbling/reaction sites were observed in the substrate, and it was speculated [17] had formed from Pb in sintering. Substrate bubbling and PZT blistering has also been found in composite sol PZT thick films sintered under an air atmosphere [9]. It has been speculated that blistering in PZT thick films on platinised silicon substrates was caused by Ti and oxygen diffusion into the Pt layer with the formation of intergranular TiO_2 [18]; however, this claim was based upon TEM evidence which was omitted from the paper in which the claim was made [18]. Further, reactive sputtering of a TiO_2 layer with subsequent direct deposition of Pt, without a Ti adhesion layer, did not result in the formation of blistering after PZT thick film fabrication [18]; the absence of blistering was attributed to the absence of available atomic Ti for diffusion. However, in another study TiO_2 barrier layers were deposited onto silicon nitride coated substrates through sputtering of Ti followed by thermal oxidation [9]; A Pt/Ti back electrode was prepared onto the TiO_2 with an annealing step to reduce compressive stresses in the back electrode. PZT thick films were then fabricated on the electrode without the formation of blisters.

This would imply that it is residual stress within the electrode and not the diffusion of atomic Ti into the electrode that gives rise to the blistering observed in PZT thick films.

The effect of high po_2 sintering of PZT on the Si substrate is unclear although SiO_2 can form under an oxidising atmosphere and flux with PbO to yield $PbSiO_3$ at 720°C (see equation (7)).

$$Pb + Si + O_2 \longleftrightarrow PbO + SiO_2 \longleftrightarrow PbSiO_3 \quad \textbf{(7)}$$

Therefore interfacial damage appears to occur both at high and low po_2 in PZT thick films prepared on platinised silicon substrates. The diffusion of Pb seems to be the principle cause of observed difficulties; consequently, blocking the diffusion of Pb is essential for reliable PZT thick film devices to be fabricated. This paper reports on the stabilisation of PZT thick films on Pt/Ti substrates and the integration of these films with silicon micromachining for application within microsystems.

Experimental

The preparation of PZT thick films has been discussed elsewhere [19] in which a PZT powder (PZ26 Ferroperm SA) was dispersed in a PZT sol yielding a slurry. It should be noted that the slurry contained a PbO-Cu_2O eutectic sintering aid 5 % by weight of PZ26 powder, the sintering aid was 86 % PbO by composition. Standard PZT thick films of the form 4[C+4S] were prepared; all layers were dried and crystallised at 200°C/50s and 450°C/15s respectively. The sol was prepared with a concentration of 1.1 M by Pb and was prepared with a 5% excess of PbO. The sol was diluted to 50 % with 2-methoxyethanol before infiltration. Layering of diluted sol between slurry layers was found to aid densification [20]. Green thick films were sintered using an AG Associates Heat Pulse 210 furnace, and were sintered with a flow rate, sintering time, and ramp rate of 30 l/min, 30 min and 30 °C/s respectively. Unless otherwise stated all films were sintered at 710 °C under Ar and prepared on platinised silicon substrates of the form: PZT/Pt/Ti/Si.

Interface analysis

PZT thick films of the form [S+7(C+S)+C] were prepared and half of the films were sintered under air and the other half of the films were sintered under Ar for 30 min. For each atmosphere the films were fired at three different temperatures: 710, 800 and 900 °C. Wafer pieces were analysed by X-ray diffraction and SEM on a Siemens D5005 X-ray Diffractometer and Cambridge Instruments ABT55 respectively. Dielectric constant and loss were measured on a Wayne Kerr 6425 precision component analyser.

KOH etching was considered as an alternative approach to DRIE for cantilever release; consequently, PZT thick films were prepared on double sided 200 nm thick Si_3N_4 coated substrates to test the usefulness of anisotropic etching. A PZT/Pt/Ti/Si_3N_4/Si film was secured to a glass support with black wax and refluxed in 20% KOH at 60 °C for 1 hour with the back face of the wafer piece exposed to the etchant. The PZT/Pt/Ti component of the film was cleaved from the substrate. EDS analysis was conducted on the surface of

the back electrode and on the exposed substrate surface to investigate interfacial composition of the cleaved layers.

Diffusion barriers

Barrier layers were prepared on both Si wafers and Si_3N_4 coated wafers. The barrier layers considered were YSZ (1 µm) and TiO_2 (300 nm). TiO_2 was prepared by sputtering Ti (200 nm) followed by thermal oxidation at 700 °C for 10 min in a Pyrotherm Box Furnace with a ramp rate of 3 °C/min. The YSZ $((YO_2)_{0.18}\ (ZrO_2)_{0.82})$ diffusion barrier layer was deposited by EB-PVD with an Electrotec Electron Beam- Ion Plating Vacuum System (CL 680) with a chamber temperature and Ar flow rate of 730 °C and 185 cm^3/min respectively. TiO_2 and YSZ deposition conditions were based on [9] and [21] respectively, and all other details are given in Table 1.

PZT thick films were prepared on platinised barrier layers on Si or Si_3N_4(200 nm)/Si, and four samples were prepared for analysis: 1. PZT/Pt/Ti/TiO_2/Si, 2. PZT/Pt/Ti/TiO_2/Si_3N_4/Si, 3. PZT/Pt/Ti/YSZ/Si and 4. PZT/Pt/Ti/YSZ/Si_3N_4/Si. Surface roughness was measured with a Vecco Dek-Tak 3 surface profiler. Film adhesion was measured with a tape test, where a positive result denotes that film material was removed from the substrate. A Phillips 2000 Focused Ion Beam (FIB) microscope was used for film-electrode-barrier-substrate interface analysis.

Wet Etching of PZT

PZT was patterned photolithographically with S1818 photoresist (conditions given in Table 2), and wet etched in HF/HCl. A standard photolithography mask containing a set of features of 200 x 200 μm^2 was used. A standard etching solution was prepared from HF(aq) 48% wt in water (Aldrich Chemicals CAS 7664-39-3) and HCl(aq) 37% wt in water (Aldrich Chemicals CAS 764701-0). The etching solution was prepared by mixing HF(aq) and HCl(aq) and diluting the solution to 0.08 M and 0.16 M respectively. The PZT was etched for 5 to 45 minutes at 50 °C before stripping the resist.

Actuator processing

The processing of device wafers involves 7 steps (see Fig 2). In this work a conventional 10 cm diameter Si wafer <100> was used. In step 2 of the process a YSZ diffusion barrier layer was deposited by EBPVD (blue line in Fig 2). A Ti/Pt back electrode was sputtered (see Table 1). A 300 nm thick Cr layer was sputtered onto the back face as a protective coating against wafer staining arising from thick film deposition (see also step 2). A 10 µm PZT thick film (yellow layer in step 3 in Fig 2) of the form $[4(C+4S)]^{710}_{Air}$, and corona polled at 115 °C, at 10 kV for 10 min.

A 300 nm Cr layer was prepared with photolithography using S1818 photoresist (conditions in Table 2), sputtering (conditions in Table 1) and lift off in acetone. A set of alignment marks were left on the back face on top of the Cr protective layer for back to front alignment for subsequent processing steps.

Step 4 of Fig 2 is the opening of vias in the PZT thick film for electrical contact to the back electrode through wet etching. Unfortunately, there was no data for the wet etching of air sintered PZT films and it was decided when fabricating devices to omit this processing step. It was envisaged that photolithography with S1818 photoresist (conditions in Table 2) with etching in HF/HCl before stripping in acetone would yield the vias. However, in the absence of a wet etching step contact to the back electrode was made through sanding away the PZT from a corner of a device with SiC paper.

Step 5 of Fig 2 is the preparation of a surface electrode through photopatterning of S1818 photoresist and sputtering of Au/Cr conditions in Table 2 and Table 1 respectively. Lift off in acetone was conducted overnight yielding the surface electrode with a set of front face alignment marks.

Step 6 of Fig 2 is the photolithographic preparation of SBX® photoresist (conditions in Table 2) on the PZT film. The resist was developed in water with high pressure washing using a SSEC Model 160 Solid State Washing Unit. Washing, drying and spinning were conducted at 1000 rpm /20 s, 1000 rpm/10 s and 2000 rpm / 20 s respectively. Device wafers were powder blasted using 15µm diameter Al_2O_3 particles at a pressure of 80 psi using a Guyson Euroblast G46 powder blaster at the central microstructure facility at RAL. After machining the SBX® was stripped with stencil remover (conditions in Table 2) yielding the stack structure shown in step 6 of Fig 2.

Following the removal of SBX®, from the PZT surface, the next stage in step 6 was the removal of Cr from the back face of the wafer. Because the surface electrode was a Au/Cr layer it was considered likely that exposure of the wafer to a Cr etch solution would be deleterious to the surface electrode; consequently, before Cr etching was started a photoresist was deposited onto the top surface of the wafer to protect the surface electrode. In step 6 the surface electrode was protected with a layer of S1818 (Table 2) while Cr was removed with a mixture of Cerium ammonium Nitrate (200 g), glacial acetic acid (35 g) and deionised water (1 L). The sample was placed in the etching solution for 15 min and exposed at 40 °C. The Cr layer has to be removed before the actuators can be released (i.e. before step 7). Step 7 involves processing on the back face of the wafer which must be clean before processing can proceed. Following the removal of the Cr layer the wafer was washed in de-ionised water and air dried before stripping the S1818 photoresist in acetone.

Step 7 of Fig 2 is the release of actuators through photolithographic patterning of AZ52142 photoresist (conditions in Table 1) and deep reactive ion etching (DRIE). Back to front alignment against the marks in the front face electrode was used. The device wafer was secured to a Si support wafer with vacuum grease before DRIE. DRIE was commenced with the STS Multiplex ASE STS35413. Cantilever thickness was controlled through varying the etch time, and the wafer was etched at a rate of 2.2 µm/min for 235 min.

Results

PZT Sintering

Graphs for dielectric constant and loss are plotted against sintering temperature and are shown in Fig 3 a and b. The dielectric constant (ε_{33}) declined as the sintering temperature was increased for films sintered under an air (high po_2) or an Ar atmosphere (low po_2). The decline in ε_{33}, between 710 and 800 °C, appears more rapid in the case of Ar sintered films. This finding is unusual in that sintering temperature was expected to increase the density, of the film, and thereby the ε_{33}. Fig 3 b shows that the dielectric loss ($\tan\delta$) increases rapidly in films sintered under Ar at higher temperatures, and that it decreases in films sintered under air. Further, the standard deviation of $\tan\delta$ becomes large for Ar sintered films as temperature is increased. These results suggest that films fired under Ar and air become electrically conducting and insulating respectively with increasing sintering temperature.

SEM fracture surfaces of films fired under Ar and air are presented in Fig 4 a to c and d to f respectively. Back electrode damage was observed to increase in proportion to the sintering temperature. Films that were fired both at 800 and 900 °C in Ar exhibited closed porosity (Fig 4 b and c); the overall thickness of these films was reduced with increasing temperature suggesting that some evaporation has taken place during sintering.

SEM fracture surfaces for films sintered under air, at 710 to 900°C are shown in Fig 4 d to f. The 710°C films have a high micro-porosity; the 800°C films appear much denser but with some closed porosity and the 900°C films are fully dense. Fig 3 a implies that the dielectric constant is inversely proportional to sintering temperature and hence the density of the thick film. However, any increase in density would result in a higher dielectric constant. The SEM fracture surfaces show increasing damage to the back electrode with increasing temperature. It is proposed that the electrode damage accounts for the decline in ε_{33} with increasing sintering temperatures and this arises from a discontinuous back electrode.

Sintering at 900 °C under air and Ar (Fig 4 c and f) shows that the Ar sintered films were porous whereas the air sintered films were dense suggesting that densification was better under an air atmosphere; this was consistent with earlier findings [20].

The XRD patterns of Ar sintered films at 710 °C to 900 °C (Fig 5 a) shows a PZT powder pattern with an additional PbO phase composed of Litharge and Massicot. There was some splitting of peaks in this spectrum. Sharp peaks were observed in the spectra of PZT thick films sintered under air at lower temperatures (Fig 5 b); peak splitting was not as apparent in these films. The broad <200> peak at 43°2θ to 45°2θ indicates that a mixture of rhombohedral and tetragonal phases were present in the infiltrated PZT thick films.

Barrier Layers

FIB images of interfaces are shown in Fig 6 a and b. PZT on YSZ/Si and TiO_2/Si barrier layers are shown. YSZ/Si is the barrier layer that exhibits the best adhesion. The PZT thick film prepared on the YSZ/Si barrier layer appears to be more porous than the film prepared on the TiO_2 based barrier layers. Although the TiO_2-barrier-layer was effective in preventing the diffusion of Pb the adhesion of the PZT/Pt/Ti/TiO_2/Si was found to be much poorer by comparison with PZT/Pt/Ti/YSZ/Si film. YSZ was chosen as the stabilisation system for PZT thick films.

Table 4 shows roughness (R_a) values for the barrier layer on the particular substrate. The PZT/Pt/Ti/YSZ film had the lowest R_a of all the barrier layers and films on barrier layers. The YSZ on Nitride barrier had the highest value of surface roughness. It was found that the greater the surface roughness of the PZT the more positive the values of the tape test: more material was removed on the tape. The Surface roughness values for PZT films on titania indicated that for the silicon nitride substrate titania was a better barrier layer than YSZ. Although YSZ/Si was the best barrier layer overall

Wet Etching of PZT

PZT was completely removed from the substrate after 14 min yielding back electrode surface. However prolonged exposure to the etching solution corroded the back electrode ultimately revealing the underlying substrate (see Fig 7). Exposure for longer periods results in the corrosion of the back electrode; in the case of films etched for >45 min the back electrode had peeled away from the substrate in places revealing the exposed Si substrate. Bubbling was observed on the exposed substrate surface. Side walls of wet etched PZT thick films exhibited roughening consistent with grain pull out (see Fig 8). This suggests preferential etching of the PZT grains at the boundary.

Cleaving of layers on Si_3N_4 support

Chemical analysis was conducted on both cleaved surfaces through EDS and is given in Table 3. Bubbling consistent with wet etched PZT (Fig 7) was found on the substrate surface. Two regions were analysed on the Si surface inside and outside the bubbling. A higher concentration of Pb was detected inside the bubbling than outside indicating the presence of lead silicate glass $PbSiO_3$ within the bubbles. Pb had diffused through the back electrode into the underlying silicon. No trace of Si_3N_4 could be found on either surface.

Integration of thick film processing route

The sol component of the slurry builds up on the wafer chuck during thick film processing and is transferred to the back face of the wafer during the various spin and

heating steps resulting in staining (see Fig 9). The image shows a Si_3N_4 wafer section staining before (Fig 9 a) and after (Fig 9 b) sintering of the wafer. The difference in coloration is attributed to the formation of $PbSiO_3$ with the substrate after sintering. Staining necessitates the deposition of a Cr protective layer before thick film deposition.

Powder blasted thick films have resulted in the cutting of near vertical PZT thick film walls (see Fig 10). Intra-grain cleavage has occurred during powder blasting; the Al_2O_3 particles appear to cut straight through the PZT of the thick film. Cavity widths ≤80 µm and > 80 µm were cut to a maximum depth of 35 µm and 40 µm respectively. This image demonstrates dense, conformal, patterned PZT thick films with a stable Si – film interface. Initially the SBX® photoresist was prepared at 50 µm and 25 µm thickness; however minimum edge shift was found to occur at a photoresist thickness of 35 µm. Maximum resolution of a 35 µm thick layer of SBX® photoresist was optimised to a line width of ≤ 50 µm; however, this was using a low pressure water supply as the developer. An unfortunate side effect of SBX® is the collection of residue in the base of photoresist cavities when developed with a low pressure water supply; the residue can only be removed with a high pressure water developing step. The residue can significantly reduce the resolution of the final cut features. The fabricated shapes in this paper were made only after developing the resist using the high pressure washing system. Unfortunately we have no data on the resolution of the resist following this high pressure step, but final cut features were found to vary ±5 µm over a length 150 µm. This would imply that following the high pressure developing step the resolution of the SBX® photoresist was significantly better than ≤ 50 µm. The smallest cut feature we have resolved had a line width of 80 µm; although it is our opinion that much smaller features are achievable.

Successful removal of the Cr layer yielded a clean back face enabling DRIE to be used for cantilever release. DRIE was used to resolve the device in Fig 11. A spiral shape was selected because of the difficulty in fabricating this shape this demonstrated versatility of this technique in fabricating complex 2D shapes.

Discussion

During the sintering of PZT thick films, Pb was found to diffuse into the substrate. The addition of a YSZ diffusion barrier minimised Pb diffusion. The TiO_2 barrier layer system was better than YSZ on Si_3N_4 coated substrates. It is considered most likely that the cleavage of the PZT and electrode from the substrate during anisotropic etching of Si resulted from the attack of KOH on the interfacial glass. As the lead silicate glass is thought to form from the diffusion of Pb during sintering, the addition of an effective barrier layer such as TiO_2 is thought to prevent its formation. If anisotropic etching is to be used for cantilever release then a TiO_2 barrier will provide greater stability for the PZT film on Si_3N_4 coated wafers; conversely, if DRIE is to be used then YSZ will provide greater stability for the PZT on a Si substrate.

Introduction of the barrier layers has meant that PZT thick films can be sintered under an air atmosphere without damage being incurred to the back electrode or film delamination

occurring. The improved densification of PZT thick films fired under air is anticipated, therefore, to improve electrical and piezoelectric properties.

Intra-granular cleavage (Fig 10) indicates that the internal structure of the PZT grains was dense, and that any porosity found in the PZT thick films appears to occur only at the grain boundaries. However, in the case of wet etched PZT, the film was preferentially etched about the grain resulting in roughened side walls. Grain pull out from bulk PZT ceramics by wet etching in concentrated HCl(aq) has been observed elsewhere [22]. Rougherning of etched side walls in thin [23] and thick [24] PZT films etched with a dilute mixture of HF(aq)/HCl(aq) has also been reported. Results reported in this paper are consistent with the literature.

The combination of processing steps yields conformal and dense PZT thick films, between 2 μm to 100 μm thick, with a low surface roughness. The PZT can be etched to reveal the back electrode, or it can be blasted through to the underlying substrate. The combination of patterning route, allows any device shape to be cut into the plane of the PZT film. Indeed, a planar PZT film on any substrate material can be patterned in this way. The exception being highly elastic materials e.g. polymers. The introduction of DRIE to release the actuators permits thickness control of the actuator substrate even if a buried oxide wafer was not used.

The coefficient of thermal expansion (CTE) of TiO_2, Si_3N_4 and SiO_2 are respectively 9.1 x 10^{-6} °C^{-1}, 3.0 x 10^{-6} °C^{-1} and 0.5 x 10^{-6} °C^{-1}; these values indicate that the mismatch between TiO_2/SiO_2>>TiO_2/Si_3N_4. Rapid thermal cycling of the PZT thick films will result in expansion variations within the different layers, and separation will occur where the difference in CTEs is greatest. Consequently, PZT/Pt/Ti/TiO_2/Si_3N_4/Si films were more stable than PZT/Pt/Ti/TiO_2/Si films: where there exists a thin SiO_2 layer on the surface of the Si at the TiO_2/Si interface. It is not clear why PZT/Pt/Ti/YSZ/Si films were more stable than PZT/Pt/Ti/YSZ/Si_3N_4/Si films.

Electrode Substrate Interface

It was proposed [3] that the intermetallic layer in Fig 1 a had formed through the reduction of PbO to Pb from the eutectic sintering aid. Atomic lead then yields an intermetallic with Pt through diffusion of atomic Pb into the back electrode. Upon saturation of Pt_3Pb continued Pb diffusion yields PtPb and the Pt_3Pb phase forms discrete islands: These islands are shown in Fig 1 a.

$$Pt_3Pb(s) + 2Pb(l) \rightarrow 3PtPb(s) \qquad \textbf{(8)}$$

Intermetallics are normally re-oxidised with the reformation of the Pt electrode. In the case of PZT thin films, the Pb reforms PbO (see equation (9)).

$$yPt_xPb(s) + \tfrac{y}{2}O_2(g) \longleftrightarrow xyPt(s) + yPbO(l) \quad \textbf{(9)}$$

Intermetallic formation was acute in films where there had been no intermittent pyrolysis of sol layers: no α2=450°C/15s treatment such as Fig 1 a. Pt_xPb formation was also acute where the sol had formed glassy layers between the composite slurry layers such as in the film shown in Fig 1 a [3]. The increased carbon content of these films, due to the absence of pyrolysis, is considered to have aided the formation of the metastable phase: lowering po_2 at the interface.

The intermetallic forms only at low po_2 and takes the values x=1 and 3. However, lead silicate glass can only form from the product of lead oxide and silica, not from atomic Pb. Pt_xPb can only form from atomic Pb and atomic Pt. The most likely explanation is that the reaction has seven stages:

1) Residual C reduces the PbO component of the sintering aid to Pb. This stage takes place in the thick film.
2) Diffusion of atomic Pb into the Pt electrode.
3) Pt_3Pb formation
4) PtPb forms with continued diffusion of Pb into the Pt back electrode
5) Excess Pb diffuses through the back electrode
6) Pb_xPt, Pb and Si are oxidised to Pt, PbO & SiO_2 respectively.
7) Fluxing of PbO and SiO_2 to yield $PbSiO_3$ glass

The lead silicate glass can form under high po_2 when in the presence of PbO(l); consequently, substituting equation (7) into equation (9), equation (10) is obtained.

$$yPt_xPb(s) + ySiO_2(s) + \tfrac{y}{2}O_2(g) \longleftrightarrow yPbSiO_3(s) + xyPt(s) \quad \textbf{(10)}$$

The lead silicate glass forms between electrode and substrate only under conditions of high po_2 when films were sintered under air. Thus, it was considered unlikely that an intermetallic phase would be observed in PZT thick films sintered under an air atmosphere where po_2 was higher.

The lead silicate glass forms under an oxidising atmosphere, with the intermetallic forming initially under low po_2 at the film electrode interface; subsequently, as po_2 increases at the interface the intermetallic would be re-oxidised yielding the Pt back electrode.

Swelling of the back electrode was observed in samples sintered under Ar at higher temperatures (in Fig 4 c). Swelling of the back electrode has also been observed in the literature [3, 16]. Sintering under an Ar atmosphere is likely to have resulted in a low interfacial oxygen partial-pressure. Glass-like layers that formed from infiltration in Fig 1 a were anticipated to have further inhibited oxygen diffusion to the interface. The low oxygen-partial-pressures that have resulted from sintering under Ar, with m>3, were

considered to have prevented the reformation of the Pt electrode. The Pt back electrode reformed through intermetallic re-oxidation. In air sintered films po_2 was sufficient for the re-oxidation of the Pt electrode. Therefore, the intermetallic phase was observed only in highly infiltrated films sintered under Ar atmospheres.

Concluding Remarks

In this paper we have sought to explain the interfacial chemical reactions occurring during the sintering and preparation of PZT thick films on platinised silicon substrates. We have proposed a seven step mechanism involving the simultaneous formation of a lead platinum intermetallic phase and the presence of a lead silicate glass phase; this mechanism is dependent both on the interfacial oxygen partial pressure and the sintering temperature. We have shown that the extent of infiltration influences delamination; infiltration is thought to result in a progressive sealing of the porous thick film against the sintering gas thereby lowering the oxygen partial pressure at the back electrode. It has been known for sometime that the intermetallic phase is stable only under reducing conditions; and a conclusion of this work is that its presence after sintering requires reducing conditions at the back electrode during the sintering stage. The formation of the intermetallic layer acts to weaken film adhesion where we have shown that the film delamination occurred at the interface between the electrode and the silicon substrate. A means of patterning and fabricating dense conformal composite PZT thick films with stable interfaces has been proposed; this was based on the novel use of a YSZ diffusion barrier coating and powder blasting.

References

1 D.A. Barrow, T.E. Petroff, and M. Sayer, Method for Producing Thick Ceramic Films by a Sol-Gel Coating Process, United States Patent No. 5,585,136, United States of America, 1996.

2 D.L. Corker, R.W. Whatmore, E. Ringgaard, and W.W. Wolny, Liquid Phase Sintering of PZT Ceramics, Journal of the European Ceramic Society, 20 (2000) 2039-2045.

3 R.D. Haigh, Ferroelectric Thick Films Prepared by Chemical Solution Deposition of Sol-Gel Composite Slurries, MSc. Thesis, Cranfield University, 2001.

4 T. Ohno, M. Kunieda, H. Suzuki, and T. Hayashi, Low-Temperature Processing of Pb(Zr-0.53,Ti-0.43)O-3 Thin Films by Sol-Gel Casting, Jpn. J. Appl. Phys. Part 1 - Regul. Pap. Short Notes Rev. Pap., 39 (2000) 5429-5433.

5 D. Xia, M. Liu, Y. Zeng, and C. Li, Fabrication and Electrical Properties of Lead Zirconate Titanate Thick Films by the New Sol-Gel Method, Materials Science and Engineering, B87 (2001) 160-63.

6 C. Zhao, Z. Wang, W. Zhu, O. Tan, and H. Hng, Microstructure and Properties of PZT53/47 Thick Films Derived from Sols with Submicron-Sized PZT Particle, Ceramics International, 30 (2004) 1925-27.

7 A.L. Kholkin, V.K. Yarmarkin, A. Wu, M. Avdeev, P.M. Vilarinho, and J.L. Baptista, PZT-Based Piezoelectric Composites via a Modified Sol-Gel Route, Journal of the European Ceramic Society, 21 (2001) 1535-1538.

8 R.A. Dorey and R.W. Whatmore, Electroceramic Thick Film Fabrication for MEMS, Journal of Electroceramics, 12 (2004) 19-32.
9 F.F.C. Duval, R.A. Dorey, R.D. Haigh, and R.W. Whatmore, Stable TiO2/Pt Electrode Structure for Lead Containing Ferroelectric Thick Films on Silicon MEMS Structures, Thin Solid Films, 444 (2003) 235-40.
10 S.A. Wilson, R.D. Haigh, J.E.A. Southin, R.A. Dorey, and R.W. Whatmore, Design of Spiral Piezoelectric Cantilever Unimorphs for Microactuation, Proceedings of the Euspen International topical conference, Aachen, Germany, 2003.
11 R.D. Haigh, Novel Piezoelectric Thick Film Actuators, Ph.D. Thesis, Cranfield University, 2006.
12 Z. Wang, W. Zhu, H. Zhu, J. Miao, C. Chao, C. Zhao, and O.K. Tan, Fabrication and Characterisation of Piezoelectric Micromachined Ultrasonic Transducers with Thick Composite PZT Films, IEEE Trans. Ultrason. Ferroelectr. Freq. Control, 52 (2005) 2289-97.
13 H. Zhu, J. Miao, Z. Wang, C. Zhao, and W. Zhu, Fabrication of Ultrasonic Arrays with 7 μm PZT Thick Films as Ultrasonnic Emitter for Object Detection in Air, Sensors and Actuators, A: Physical, 123-124 (2005) 614-19.
14 Q.-M. Wang and L. Eric Cross, Analysis of High Temperature Reduction Processing of RAINBOW Actuator, Materials Chemistry and Physics, 58 (1999) 20-25.
15 K.G. Brooks, I.M. Reaney, R.D. Klissurska, Y. Huang, L. Bursill, and N. Setter, Orientation of Rapid Thermally Annealed Lead Zirconate Titanate Thin Films on (111) Pt Substrates, Journal of Materials Research, 9 (1994) 2540-53.
16 S.P. Beeby, A. Blackburn, and N.M. White, Processing of PZT Piezoelectric Thick Films on Silicon for Microelectromechancial Systems, Journal of Micromechanics and Microengineering, 9 (1999) 218-229.
17 P. Glynne-Jones, S.P. Beeby, P. Dargie, T. Papakostas, and N.M. White, An Investigation into the Effect of Modified Firing Profiles on the Piezoelectric Properties of Thick-Film PZT Layers on Silicon, Meas. Sci. Technol., 11 (2000) 526-531.
18 Z. Wang, J. Miao, and W. Zhu, Piezoelectric Thick Films and Their Application in MEMS, Journal of the European Ceramic Society, 27 (2007) 3759-64.
19 D.L. Corker, Q. Zhang, R.W. Whatmore, and C. Perin, PZT 'Composite' Ferroelectric Thick Films, Journal of the European Ceramic Society, 22 (2002) 383-390.
20 R. Dorey, R.D. Haigh, S.B. Stringfellow, and R.W. Whatmore, Effect of Sol Infiltrations on the Electrical Properties of PZT, Proceedings of Ferroelectrics UK, Sheffield University, UK, 2001.
21 T. Matthee, J. Wecker, H. Behner, and G. Friedel, Orientation Relationships of Epitaxial Oxide Buffer Layers on Silicon <100> for High Temperature Superconducting YBa2Cu3O7-x Films, Journal of Applied Physics Letters, 61 (1992) 1240-2.
22 S.E. Trolier, C. Xu, and R.E. Newnham, A Modified Thickness Extensional Disk Transducer, IEEE Transactions on Ultrasonics, Ferroelectrics,and Frequency Control, 35 (1988) 839-42.
23 W. Liu, J. KO, and W. Zhu, Device Patterning of PZT/Pt/Ti/ Thin Films on SiO2/Si3N4 Membrane by a Chemical Wet Etching Approach, Journal of Material Science Letters, 19 (2000) 2263-5.
24 R.A. Miller and J.J. Bernstein, A Novel Wet Etch For Patterning Lead Zirconate-Titanate (PZT) Thin Films, Integr. Ferroelectr., 29 (2000) 225-231.

Tables

Table 1 Conditions used for the deposition of thin films by vacuum techniques. It should be noted that the sputtering pressure for all samples was 0.001 Torr

Table 2 Photoresist deposition and photopatterning conditions

Table 3 Chemical analysis by EDS of cleaved interfacial layers following attempted KOH anisotropic etching of Silicon support.

Table 4 Surface roughness data of both barrier layers and PZT thick films. Barrier layers and thick films have been prepared on differing substrates, and the PZT thick films were prepared on platinised barrier layers.

Illustrations

Fig 1 SEM polished cross sections of PZT thick films of the form: (a) $[S+7(C+5S)+C]^{710}{}_{Ae}$/Pt/Ti/Si (Top) and (b) $[S+7(C+S)+C^2]^{710}{}_{Ar}$/Pt/Ti/Si (bottom). Images were taken from Haigh [3] and reproduced with kind permission.

Fig 2 Process flow for the fabrication of PZT thick film unimorphs

Fig 3 Effect of thermal treatment and sintering atmosphere on the relative permittivity (a) and dielectric loss (b) of infiltrated PZT thick films. Error bars were determined from the standard deviation of measurements for each point. The error in tanδ at 710 °C (air sintered) is present but too small to be visible on the graph.

Fig 4 SEM fracture surfaces of PZT thick films sintered between 710 °C to 900 °C under atmospheres of Ar and air. The images show a progressive increase in density with firing temperature when fired under air (a-c). However, Ar sintered films exhibit pore coalescence as sintering temperature is increased (d-f).

Fig 5 XRD spectra of Ar sintered films (a) and air sintered films (b). The spectra show the effect of sintering temperature. The Ar sintered film shows a second phase. In the Fig Per, Mas and Lit correspond to perovskite (PZT), Massicot (PbO) and litharge (PbO) respectively.

Fig 6 FIB image of a PZT/Pt/Ti/YSZ/Si film showing stabilisation of substrate system against delamination (a). FIB Image of a PZT/Pt/Ti/TiO_2/Si showing some separation from the substrate (b). Image sampled at 45 ° to normal.

Fig 7 Wet etched PZT thick film fully etched to reveal exposed back electrode after 45 min exposure to HF/HCl. The Pt is badly corroded and bubbling can be observed in the underlying substrate.

Fig 8 Sidewall SEM of wet etched PZT, looking down from an angle of 30 ° from normal. This shows that the sidewall is quite rough and that grains have been removed preferentially from the grain boundary.

Fig 9 Back face of wafer after PZT thick film deposition showing significant staining of the wafer with sol from the composite slurry. Left wafer before sintering (a) and right after sintering (b).

Fig 10 SEM micrograph of a powder blasted thick film. The micrograph shows the cut-face of the PZT thick film. The picture was taken at a 30 ° angle, relative to the normal, to observe the cut sidewall.

Fig 11 Plan view of released spiral actuator

Acknowledgements
The authors acknowledge the financial assistance of The Engineering & Physical Sciences Research Council (EPSRC) grant No GR/N34017. and BAe Systems (Sowerby Research Centre). We wish to thank Dr Q. Zhang, Dr. C. Shaw of Cranfield University for the preparation of PZT etching solutions and the DRIE release of cantilevers respectively. We also wish to thank Dr. B. Stevens at Rutherford Appleton Laboratory for his assistance with powder blasting.

Roger Whatmore received the Ph.D. degree from Cambridge University, Cambridge, U.K., in 1976. He was with the Cavendish Laboratory, Cambridge University, where he conducted original research into the structure and phase transitions in low-Ti content Pb(Zr,Ti)O3 solid solutions. In 1976, he joined GEC Marconi Materials Technology (formerly Plessey Research), Caswell, U.K., where he was involved with the applications of ferroelectric materials to piezoelectric, pyroelectric, and electrooptic devices. In October 1994, he took up the Royal Academy of Engineering Chair in Engineering Nanotechnology at Cranfield University, Cranfield, Bedford, U.K. In 2006 he moved to The Tyndell Institute in Cork Ireland where he is currently CEO.

Richard Haigh obtained his BSc. (Hons) in Chemistry from the University of Surrey in 1998. He obtained his Ph.D in Materials Science and Applied Physics in 2006 from Cranfield University, in Bedfordshire UK, where he worked on the development of thick film piezoelectric materials for actuators. He is currently at the Open University, in Milton Keynes UK, where he is working on the determination of residual stresses of nuclear materials using neutron and synchrotron diffraction. His current interests also include imaging of creep cavitation damage.

Target	Type	Electrical conditions	Deposition Rate / nm/s	Thickness / nm	Vacuum pressure / Torr	Purpose
Cr	RF Sputtering	200 W	1.60	300	5×10^{-7}	Back face protection
Cr	RF Sputtering	200 W	1.60	5	5×10^{-7}	Adhesion layer (Au)
Au	RF Sputtering	100 W	0.42	100	5×10^{-7}	Surface electrode
Ti	RF Sputtering	300 W	0.29	200	5×10^{-7}	Diffusion barrier
Ti	RF Sputtering	300 W	0.29	8	5×10^{-7}	Adhesion layer (Pt)
Pt	DC Sputtering	0.725 A at 425 V	1.72	200	5×10^{-7}	Back electrode
YSZ (Melt)	EB-PVD	10 kV at 0.45 A	25.0	1000	7.0×10^{-3}	Diffusion Barrier

Photoresist	S1818 (Shipley Europe Ltd)	AZ52142 (Clariant)	SBX (PhotoBrasive Systems)
Spin Speed	4000 rpm / 60 s	2000 rpm / 40 s	-
Drying time	-		24 hours
Soft bake	115 °C/ 90 s	90 °C / 110 s	-
Thickness	-	-	35 μm
Exposure time	15 s	25 s	25 s
Developer	MF319 (Shipley Europe Ltd)	25% AZ351B (Clariant)	Water
Development time	75 s	260 s	20 s
Drying time	-	-	10 s
Stripping reagent	Acetone	Acetone	25% stencil remover (Absolute Screen Ltd.).

	Element / Atomic %								
Layer analysed	C	O	Si	K	Ti	Cu	Nb	Pt	Pb
PZT Film & Back Electrode	n.d.	23.43	n.d.	6.61	7.68	4.38	2.48	42.28	13.15
Substrate region 1	29.56	21.96	45.21	2.87	n.d.	n.d.	n.d.	n.d.	0.40
Substrate region 2	n.d.	53.21	27.38	13.41	n.d.	n.d.	n.d.	n.d.	6.00

Barrier Layer	Substrate surface	Ra Barrier layer / nm	Ra Thick film / nm	Tape test
YSZ	Si	5	73	Negative
YSZ	Si_3N_4	-	594	Positive
TiO_2	Si	25	147	Positive
TiO_2	Si_3N_4	21	71	Positive
Standard	Si_3N_4	-	1080	Positive

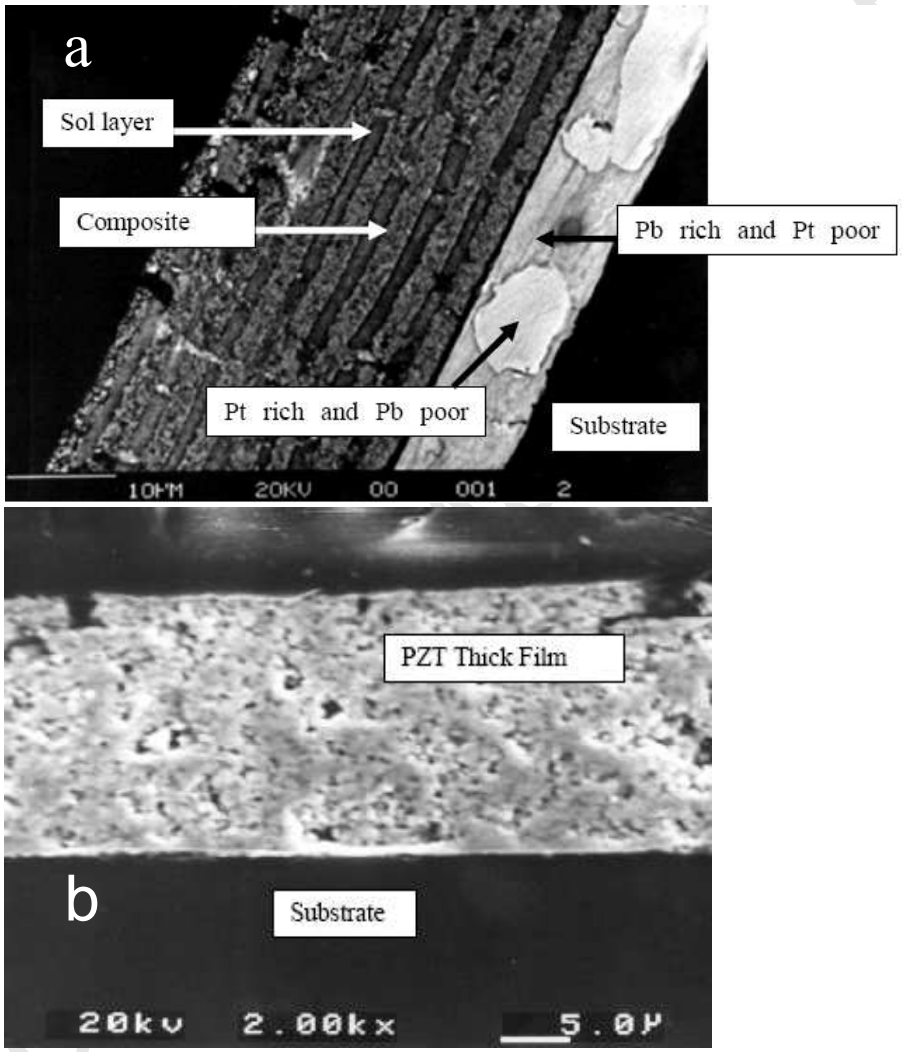

1

2

3

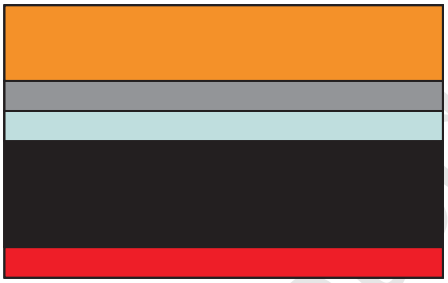

4

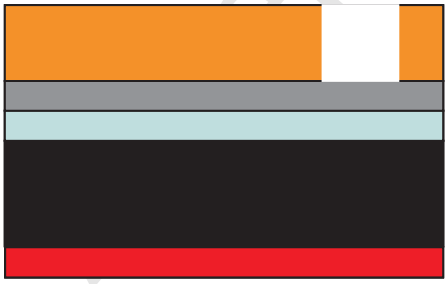

5

6

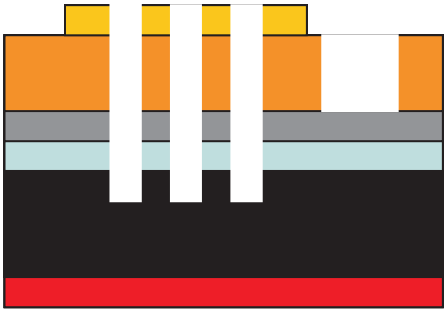

7

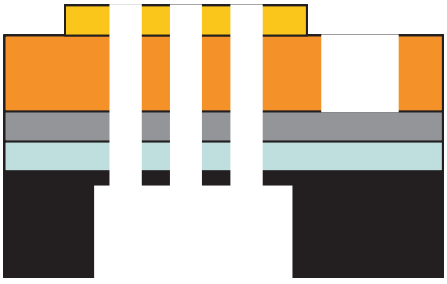

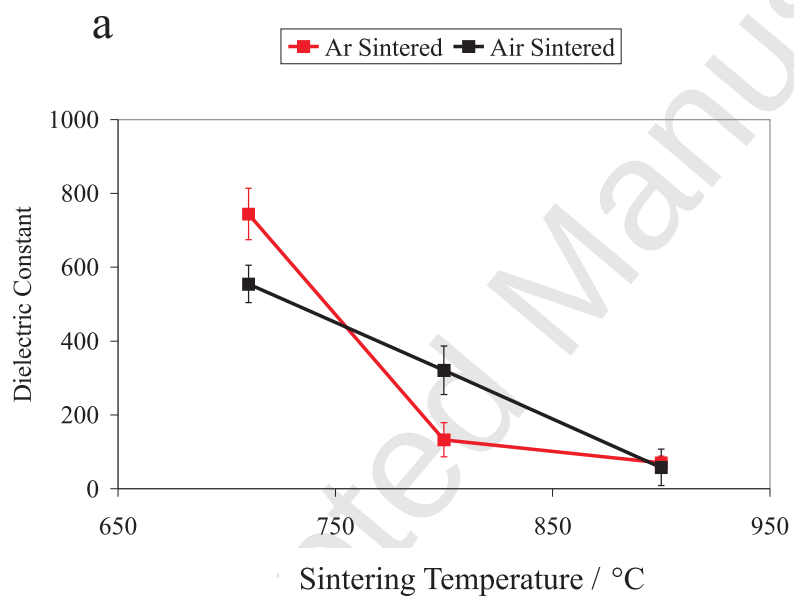

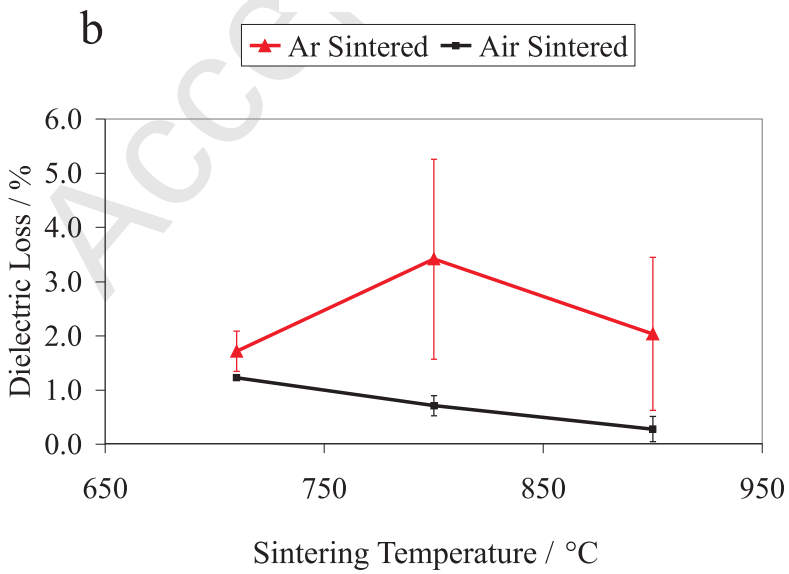

Ar fired Films

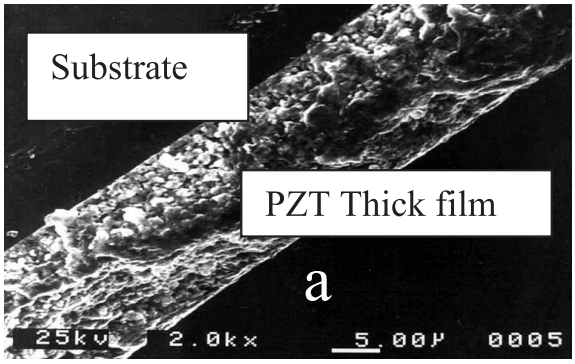

710°C

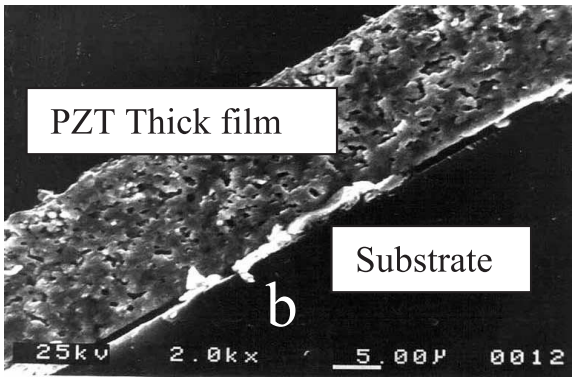

800°C

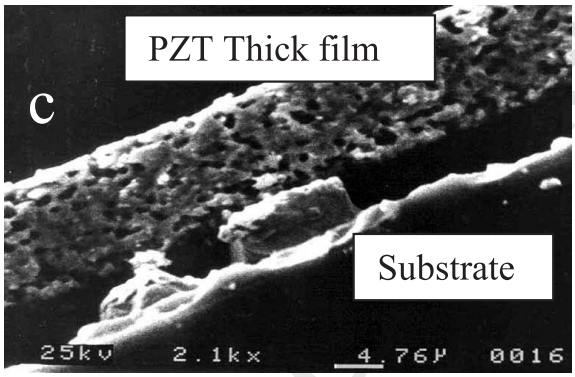

900 °C

Air Fired Films

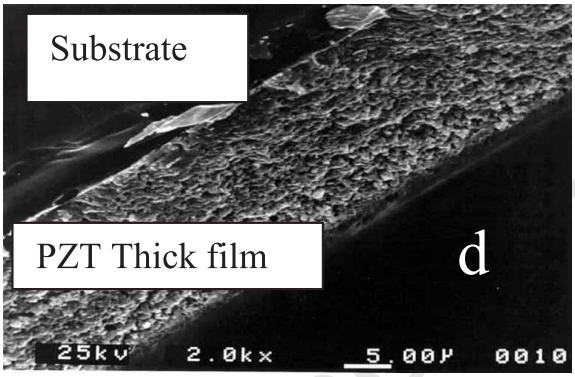

710°C

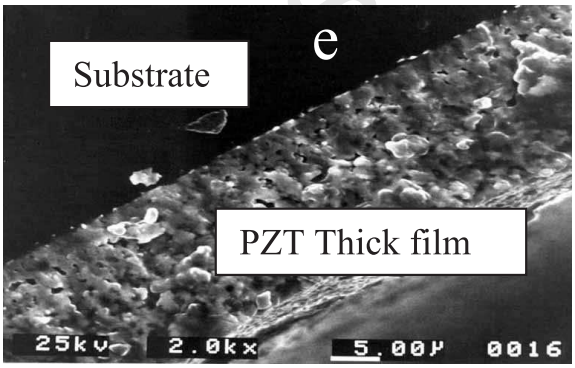

800°C

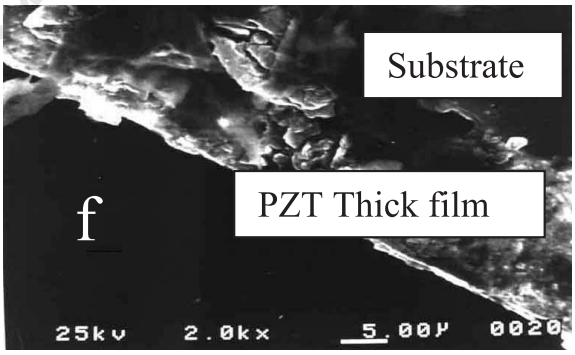

900 °C